CrossMark

ORIGINAL ARTICLE

Fast calibration of electromagnetically tracked oblique-viewing rigid endoscopes

Xinyang Liu[1] · Christina E. Rice[1,2] · Raj Shekhar[1]

Abstract

Purpose The oblique-viewing (i.e., angled) rigid endoscope is a commonly used tool in conventional endoscopic surgeries. The relative rotation between its two moveable parts, the telescope and the camera head, creates a rotation offset between the actual and the projection of an object in the camera image. A calibration method tailored to compensate such offset is needed.

Methods We developed a fast calibration method for oblique-viewing rigid endoscopes suitable for clinical use. In contrast to prior approaches based on optical tracking, we used electromagnetic (EM) tracking as the external tracking hardware to improve compactness and practicality. Two EM sensors were mounted on the telescope and the camera head, respectively, with considerations to minimize EM tracking errors. Single-image calibration was incorporated into the method, and a sterilizable plate, laser-marked with the calibration pattern, was also developed. Furthermore, we proposed a general algorithm to estimate the rotation center in the camera image. Formulas for updating the camera matrix in terms of clockwise and counterclockwise rotations were also developed.

Results The proposed calibration method was validated using a conventional 30°, 5-mm laparoscope. Freehand calibrations were performed using the proposed method, and the calibration time averaged 2 min and 8 s. The calibration accuracy was evaluated in a simulated clinical setting with several surgical tools present in the magnetic field of EM tracking. The root-mean-square re-projection error averaged 4.9 pixel (range 2.4–8.5 pixel, with image resolution of 1280 × 720) for rotation angles ranged from −40.3° to 174.7°.

Conclusions We developed a method for fast and accurate calibration of oblique-viewing rigid endoscopes. The method was also designed to be performed in the operating room and will therefore support clinical translation of many emerging endoscopic computer-assisted surgical systems.

Keywords Camera calibration · Single-image calibration · Oblique-viewing endoscope · Electromagnetic tracking · Augmented reality · Computer-assisted surgery

✉ Raj Shekhar
rshekhar@childrensnational.org

1 Sheikh Zayed Institute for Pediatric Surgical Innovation, Children's National Health System, 111 Michigan Avenue NW, Washington, DC 20010, USA

2 Department of Mechanical and Aerospace Engineering, Princeton University, Princeton, NJ 08544, USA

Introduction

Computer-assisted surgery (CAS) is increasingly an integral part of modern patient care. A key capability to enable and expand CAS approaches in endoscopy is the calibration of the rigid endoscope, a process that includes camera calibration and hand-eye calibration (a concept that originates from robotics). Through camera calibration, intrinsic parameters (focal length, principal point, etc.) and distortion coefficients of the camera are determined [1–4], whereas hand-eye calibration produces the rigid transformation between the camera lens and the tracking device attached to the camera [5]. Endoscope calibration is critical to many CAS applications, including the emerging augmented reality (AR) application, a topic of great interest to our team. In AR, virtual models or tomographic images are overlaid on live endoscopic video to enhance intraoperative visualization. To accomplish this,
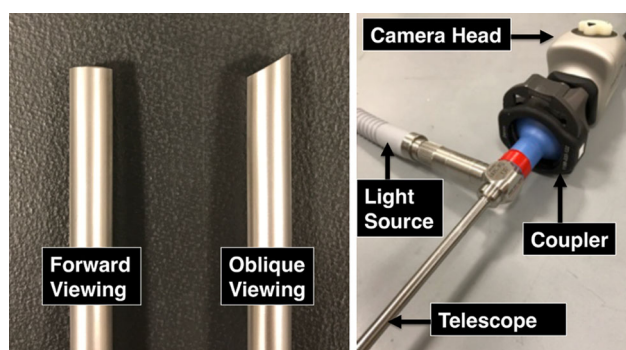
Springer

Fig. 1 *Left* imaging tips of forward- and oblique-viewing rigid endoscopes. *Right* components of a conventional laparoscope

most reported AR systems rely on external tracking, such as optical tracking [6–8] and electromagnetic (EM) tracking [9,10].

Two types of rigid endoscopes are common: (1) the forward-viewing endoscope that has a flat lens relative to the camera and (2) the oblique-viewing endoscope that has an angled (30° or 70°) lens relative to the camera (Fig. 1). An angled endoscope has the advantage of offering a much larger field of view through the rotation of its telescope relative to the camera head. However, this rotation also creates a rotation offset between the actual object shown in the camera image and the projected object obtained using the calibrated parameters before rotation (i.e., initial calibration). Although numerous calibration methods for standard camera have been reported, only a countable few groups have developed methods to calibrate oblique-viewing endoscopes and update the initial calibration result after a rotation. A key step in such methods is to track the relative rotation between the two moveable parts of the endoscope. Yamaguchi et al. [11] attached one optical marker on the telescope and another optical marker and a rotary encoder on the camera head to track this rotation. They treated the optical marker on the camera head as the reference, and, in their calibration method, the image plane was fixed. Wu et al. [12] improved the Yamaguchi method by removing the rotary encoder and treating the optical marker on the telescope as the reference. In their method, the hand-eye calibration is preserved during rotation, but the camera image rotates about the rotation center in the image plane. Similarly, De Buck et al. [13] and Feuerstein et al. [14] attached two optical markers on the telescope and the camera head to determine the rotation axis and the rotation angle. De Buck et al. further extended the standard camera model by incorporating functions that accounted for the rotation of the endoscope. The parameters of the functions were obtained by interpolation of a set of previously calculated parameter values. Different from the approaches that rely on external markers, Melo et al. [15] presented a method that used information in the camera image to calculate the rotation center and the rotation angle.

There are several limitations associated with the aforementioned approaches. First of all, optical tracking is not ideal for all clinical applications. The 6-degrees-of-freedom (DOF) optical marker usually has a relatively bulky cross- or star-shaped rigid body with several infrared reflective spheres (or LEDs) mounted on its corners. Both markers on the endoscope maintaining a line-of-sight with the optical camera during the rotation require a bulky configuration of the assembled endoscope, as well as a large physical space for surgeons to perform the rotation. This makes optical tracking challenging in a clinical setting. Second, to obtain the initial calibration, most prior approaches relied on conventional camera calibration methods [1–4], which require acquisition of multiple (typically 15 or more) images to achieve an acceptable calibration result. This lengthy calibration procedure limits their use in the operating room (OR). The only exception, to our knowledge, is the work of Melo et al. [15], in which the authors used a new method, called single-image calibration (SIC) [16], to initialize the calibration of oblique-viewing endoscopes. Although clinically feasible, the Melo method focused only on calibrating camera intrinsic parameters and distortion coefficients. Therefore, it cannot be used directly in applications such as AR because of the missing hand-eye calibration and external tracking. Third, there is not a universally accepted method to estimate the rotation center in the camera image. Wu et al. [12] assumed the principal point to be the rotation center in the image. However, this is generally not true, as demonstrated by Melo et al. [15], who estimated the rotation center using image features such as the circular image boundary contour and the triangular mark on the image boundary of an oblique-viewing arthroscope. However, these image features are not universally available. For example, most camera images produced by conventional laparoscopes do not show these features.

The purpose of this work was to develop a fast calibration method suitable for OR use for oblique-viewing rigid endoscopes. In our earlier work [17], we developed a fast calibration method for forward-viewing endoscopes using the SIC method [15,16] and EM tracking. EM tracking reports the location and orientation of a small (∼1 mm diameter) wired sensor inside the magnetic field (i.e., working volume) created by the tracking system's field generator (FG) [18]. We have extended our previous work to oblique-viewing endoscopes here by mounting two EM sensors, one on the telescope and another on the camera head, thus creating an overall compact configuration. We further developed a SIC plate that can be sterilized for clinical use. In addition, we extended the work of Wu et al. [12] by incorporating SIC and a new method to estimate rotation center in the camera image. Formulas for updating the camera matrix in terms of clockwise and counterclockwise rotations were also developed. Finally, the proposed calibration method was evaluated in a simulated clinical setting.

Materials and methods

Related work

We first briefly review the approach of Wu et al. [12], on which our calibration method is based. Wu et al. attached two optical markers on the endoscope, one on the telescope (OM_1) and another on the camera head (OM_2). They used OM_1 as the reference because it has a fixed geometric relation with the scope lens, so that the hand-eye calibration is preserved during the rotation. Let p_{OM_2} be an arbitrary point in OM_2's coordinate system. Its coordinates in OM_1's coordinate system can be expressed as

$$p_{OM_1} = {}^{OM_1}T_{OT} \cdot {}^{OT}T_{OM_2} \cdot p_{OM_2} \tag{1}$$

where OT refers to the optical tracker and ${}^B T_A$ represents the transformation from A to B.

When rotating the two optical markers relative to each other, p_{OM_2}'s corresponding coordinates in OM_1's coordinate system at various time points are recorded, forming a set of points $P_{OM_1} = \left\{ p_{OM_1}^{t_1}, p_{OM_1}^{t_2}, \ldots, p_{OM_1}^{t_n} \right\}$ where t_i is the ith time point. The points in P_{OM_1} should reside on a circle centered at the rotation center in OM_1's coordinate system O_{OM_1}. For any three points in P_{OM_1}, O_{OM_1} can be estimated based on the geometric formulas provided in [12]. To improve accuracy and robustness, Wu et al. introduced a RANSAC algorithm to, repetitively, select three random points in P_{OM_1} and calculate O_{OM_1}. For each iteration, the distances between the calculated O_{OM_1} and all points (except the three points used to calculate O_{OM_1}) in P_{OM_1} were calculated. Among all iterations, the O_{OM_1} that generates the smallest variance of those distances is chosen as the optimum rotation center. Once O_{OM_1} is obtained, it is relatively straightforward to calculate the rotation angle given the tracking data before and after the rotation.

EM tracking mounts

As mentioned before, optical tracking-based approaches may not be practical for clinical use. As shown in Fig. 2a, b, the 6-DOF optical marker is relatively bulky in size, and maintaining a line-of-sight with the infrared camera for both markers is challenging and even impossible for certain rotation angles.

In this work, we used a conventional 2D laparoscopic camera (1188 HD, Stryker Endoscopy, San Jose, CA, USA) with a 30° 5-mm telescope, and an EM tracking system with a tabletop field generator (FG) (Aurora, Northern Digital Inc., Waterloo, ON, Canada) and two 6-DOF EM sensors. The tabletop FG is specially designed for OR applications. It is positioned between the patient and the surgical table
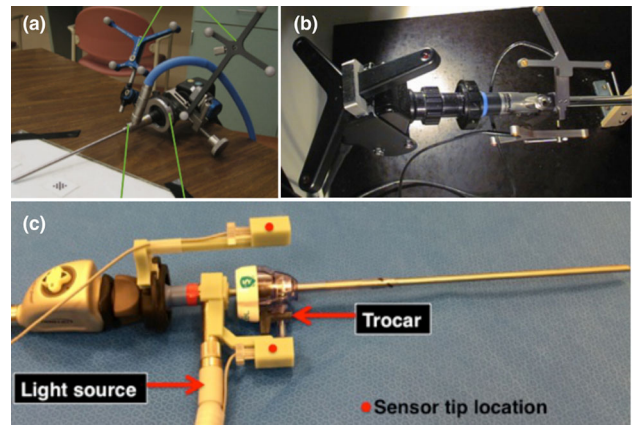

Fig. 2 a, b Optical tracking-based configurations in [12,13], respectively (reproduced with permission). **c** EM tracking mounts for a conventional 30° 5-mm laparoscope, placed within a 5-mm trocar

and incorporates a shield that suppresses distortions to the magnetic field caused by metallic materials below the FG. A recent study showed that the tabletop arrangement could reduce EM tracking error in a clinical environment [19]. As shown in Fig. 2c, we designed and 3D printed (using ABS material) two EM tracking mounts, which can be tightly snapped on the camera head and the telescope/light source, respectively.

In our design, we tried to place the two sensors as far away from the camera head as possible because the camera head causes greater distortion error in EM tracking compared with the telescope. Please refer to our previous works [10,20] for detailed measurement of EM tracking accuracy when placing the sensor near the laparoscope. During an actual surgery, the camera head is usually positioned higher than the scope lens relative to the patient. Therefore, our designed sensor locations are close to the FG as much as possible without touching the patient. As shown by Nijkamp et al. [21], this configuration yields the best tracking accuracy and stability. Because the sensors and the mounts are sterilizable and will be kept outside the patient's body, the safety issues associated with clinical use can be managed relatively easily. Compared with optical tracking-based approaches, our approach has the advantages of a much more compact configuration, no concerns regarding a loss of the line-of-sight, and a greater range of possible rotation. It should be noted that there is a small inaccessible rotation angle range (33.5° out of 360°) in our design, which is caused by the light source cable physically blocking the tracking mount on the camera head (please refer to the "Discussion" section for more details on this subject).

Clinical *fCalib*

A contribution of this work is that we have incorporated the SIC method into the calibration framework for

oblique-viewing endoscopes. In our previous work [17], we developed a fast calibration method called *fCalib* for forward-viewing endoscopes. The method combines the SIC method [15,16] (Perceive3D, Coimbra, Portugal), which estimates camera intrinsic parameters and distortion coefficients, and the conventional hand-eye calibration so that the complete calibration can be achieved by acquiring a single image of an arbitrary portion of the target pattern. In our earlier work [17], we glued a calibration pattern printed on paper on a plastic plate as a temporary solution. In this work, we have developed a clinical *fCalib* plate by laser-marking the calibration pattern on Radel® polyphenylsulfone, a type of heat and chemical-resistant polymer. As shown in Fig. 3, a 6-DOF EM sensor was permanently embedded in the plate. A tube phantom was fixed on the plate and was registered with the sensor. The tube is used for quick visual evaluation of the calibration accuracy by overlaying a virtual tube model on the camera image and comparing it with the actual tube shown in the camera image. Please refer to [17] for details of the calibration and evaluation methods associated with *fCalib*. The clinical *fCalib* plate can be sterilized using autoclave, which is necessary for fast endoscope calibration in the OR.

Calibration steps

When the telescope is stationary and only the camera head is rotated (this can be achieved by translation between coordinate systems according to Eq. 1), the camera image rotates about a point in the image plane, i.e., the rotation center in the image O_{IMG}. Wu et al. [12] assumed the calibrated principal point $C = (C_x, C_y)$ to be O_{IMG}. However, this is not gener-
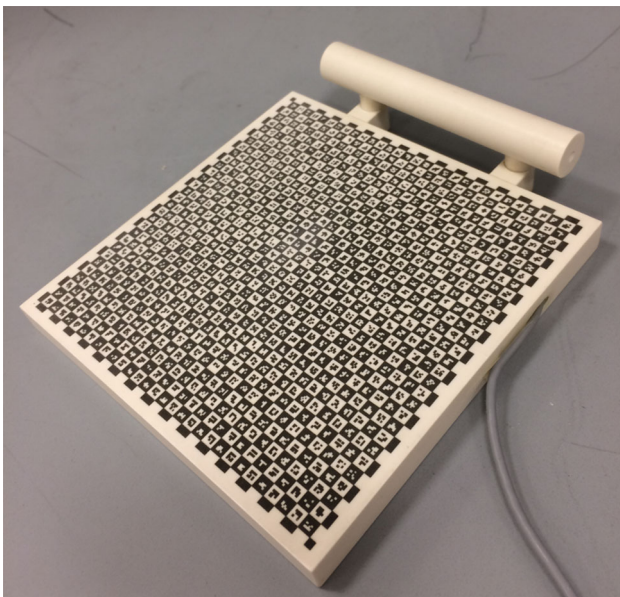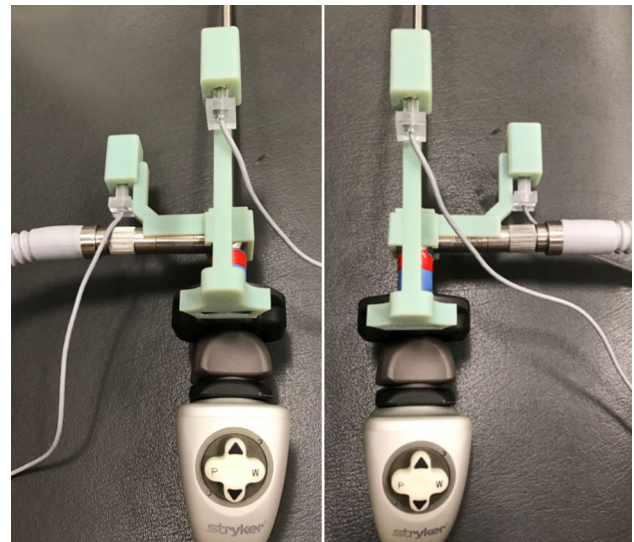

Fig. 3 Clinical *fCalib* plate

Fig. 4 Relative rotation of approximately 180° between the telescope and the camera head

ally true as explained in [15], in which the authors showed that the principal point also rotates about O_{IMG} while rotating the camera head relative to the telescope. Let $C(0°)$ be the principal point calibrated at an initial state. A generic estimation of O_{IMG} would be the midpoint of the line segment connecting $C(0°)$ and $C(180°)$, i.e.,

$$O_{\text{IMG}} = \frac{C(0°) + C(180°)}{2} \tag{2}$$

where $C(180°)$ is the principal point estimated after a relative rotation of 180° from the initial state (Fig. 4). With the use of *fCalib*, this can be achieved relatively fast and easily. Based on this estimation of O_{IMG}, we developed the following calibration method:

(1) *Obtain the rotation center in EMS$_1$'s (EM sensor on the telescope) coordinate system O_{EMS_1}*. This can be achieved using the Wu method [12] as described in the "Related work" section. In particular, we recorded EM tracking data at a frequency of 12 Hz for 15 s while rotating the camera head relative to the telescope. This yielded a total of 180 sample points located on a circle centered at O_{EMS_1} (after applying Eq. 1). We calculated O_{EMS_1} using the RANSAC algorithm with 2000 loops. The net calculation time for calculating O_{EMS_1} was <0.5 s.

(2) *Obtain the first calibration using fCalib and record the current poses of the two sensors (Pose 1)*. Calibration results include camera intrinsic parameters, distortion coefficient, and extrinsic parameters (results of the hand-eye calibration). Root-mean-square (RMS) re-projection error associated with the calibration results

was recorded. As reported in [17], the average time of calibration using *fCalib* was 14 s.

(3) *Rotate the endoscope* 180° *from Pose 1* (Fig. 4). Given O_{EMS_1} obtained in Step 1 and Pose 1 obtained in Step 2, any relative rotation angle θ from Pose 1 can be calculated. Because it is not possible to manually rotate exactly 180° from Pose 1, we considered $\theta \in [175°, 185°]$ to be a good candidate, which can often be achieved through one or two adjustments of the rotation.

(4) *Obtain the second calibration using fCalib, record Pose 2, and calculate O_{IMG} according to Eq.* 2. This completes the calibration. Between the two calibrations, the one with the smaller RMS re-projection error will be set as the Initial Calibration and its pose will be set as the Initial Pose.

After the calibration, the rotation angle θ can be calculated based on O_{EMS_1} and the Initial Pose. The camera matrix can then be updated based on θ, O_{IMG}, and the Initial Calibration. The calibration method was implemented using C++ on a laptop computer with 4-core 2.9 GHz Intel CPU and 8 GB of memory. OpenCV (Intel Corp., Santa Clara, CA, USA) functions and Perceive3D's SIC software were incorporated into the calibration software. It should be noted that the extrinsic parameters and distortion coefficient are not supposed to change with rotation.

Updating the camera matrix

In this section, we describe the formulas for updating the camera matrix with respect to clockwise (i.e., generating a clockwise rotation in the camera image) and counterclockwise rotations. Let (x_d, y_d) be the normalized pinhole projection after lens distortion, and (x_p, y_p) be its corresponding pixel coordinates in the image. We have

$$\begin{bmatrix} x_p \\ y_p \\ 1 \end{bmatrix} = K \begin{bmatrix} x_d \\ y_d \\ 1 \end{bmatrix} \tag{3}$$

where K is the camera matrix and can be simplified as

$$K = \begin{bmatrix} f_x & 0 & C_x \\ 0 & f_y & C_y \\ 0 & 0 & 1 \end{bmatrix} \tag{4}$$

where f_x and f_y are the focal lengths and C is the principal point. We assume the camera is skewless, which is often the case for endoscopes. Let $O_{\text{IMG}} = (O_x, O_y)$ be the rotation center in the image, and R_θ^+ be the conventional counterclockwise rotation matrix (we defined the counterclockwise rotation to be positive). Thus, the corrected projection after a counterclockwise rotation of θ about O_{IMG} can be expressed as

$$\begin{bmatrix} x_c \\ y_c \\ 1 \end{bmatrix} = R_\theta^+ \begin{bmatrix} x_p - O_x \\ y_p - O_y \\ 1 \end{bmatrix} + \begin{bmatrix} O_x \\ O_y \\ 1 \end{bmatrix}$$

$$= \begin{bmatrix} \cos\theta & -\sin\theta & 0 \\ \sin\theta & \cos\theta & 0 \\ 0 & 0 & 0 \end{bmatrix} \begin{bmatrix} f_x x_d + C_x - O_x \\ f_y y_d + C_y - O_y \\ 1 \end{bmatrix}$$

$$+ \begin{bmatrix} O_x \\ O_y \\ 1 \end{bmatrix}$$

$$= \begin{bmatrix} \cos\theta & -\sin\theta & (1-\cos\theta)\,O_x + \sin\theta \cdot O_y \\ \sin\theta & \cos\theta & -\sin\theta \cdot O_x + (1-\cos\theta)\,O_y \\ 0 & 0 & 1 \end{bmatrix}$$

$$\cdot \begin{bmatrix} f_x & 0 & C_x \\ 0 & f_y & C_y \\ 0 & 0 & 1 \end{bmatrix} \begin{bmatrix} x_d \\ y_d \\ 1 \end{bmatrix}$$

$$= R_{\theta, O_{\text{IMG}}}^+ K \begin{bmatrix} x_d \\ y_d \\ 1 \end{bmatrix}$$

Similarly, the rotation matrix for the clockwise rotation can be expressed as

$$R_{\theta, O_{\text{IMG}}}^- = \begin{bmatrix} \cos\theta & \sin\theta & (1-\cos\theta)\,O_x - \sin\theta \cdot O_y \\ -\sin\theta & \cos\theta & \sin\theta \cdot O_x + (1-\cos\theta)\,O_y \\ 0 & 0 & 1 \end{bmatrix} \tag{5}$$

For implementation, it is straightforward to use the above formulas for correcting rotation offset, i.e., by multiplying $R_{\theta, O_{\text{IMG}}}^+$ or $R_{\theta, O_{\text{IMG}}}^-$ on the left of the initial camera matrix.

Let p_{EMS_2} be an arbitrary point in EMS$_2$'s (EM sensor on the camera head) coordinate system, and $p_{\text{EMS}_1}^{\text{initial}}$ be its corresponding coordinates in EMS$_1$'s coordinate system at the Initial Pose. After a new rotation, the corresponding coordinates of p_{EMS_2} in EMS$_1$'s coordinate system changes to p_{EMS_1}. The direction of rotation (clockwise or counterclockwise) can be determined according to

$$\text{sgn}\left(\left[\left(O_{\text{EMS}_1} - p_{\text{EMS}_1}^{\text{initial}}\right) \times \left(O_{\text{EMS}_1} - p_{\text{EMS}_2}\right)\right]_z\right) \tag{6}$$

where O_{EMS_1} is the obtained rotation center in EMS$_1$'s coordinate system.

Experiment 1

We first evaluated our method to obtain the rotation center in the image O_{IMG}. After attaching the EM tracking mounts, a team member repetitively performed five freehand calibrations following the described calibration steps (Steps 1–4), and the results of these calibration trials were recorded and

analyzed. The starting relative angle between the two parts of the laparoscope was gradually increased approximately 30°−40° between two consecutive calibration trials. When acquiring images, the distance between the laparoscope lens and the center of the *fCalib* plate ranged from 7 to 9 cm, which fell in the typical distance range when using such a laparoscope clinically.

Experiment 2

In Step 3 of our calibration method, we require a rotation of 180° ± 5° from Pose 1 to yield Pose 2. To investigate the influence of violation to this rule, we performed additional calibration trials, in which the rotation angles between Pose 1 and Pose 2 were approximately 170°, 160° and 150°.

Experiment 3

We subsequently validated the static calibration accuracy of the proposed method. Because EM tracking accuracy is susceptible to the presence of metallic and conductive materials, we performed experiments in a simulated clinical environment, as shown in Fig. 5. The tabletop EM FG was placed on a surgical table. A plastic laparoscopic trainer that simulates patient's abdomen was placed on the FG. Two common laparoscopic surgical tools, one grasper and one pair of scissors, were inserted into the trainer through trocars. To simulate the use of a laparoscope in an ultrasound-based AR system, a laparoscopic ultrasound (LUS) probe was inserted into the trainer. The LUS probe was connected to the ultra-
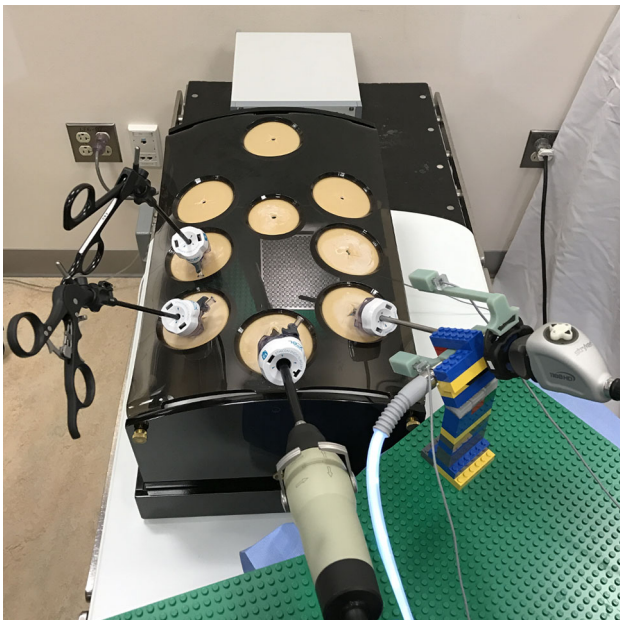

Fig. 5 Simulated clinical environment for validation of calibration accuracy

sound scanner, and the scanner was kept on throughout the experiments. The *fCalib* plate was placed inside the trainer and was used only for the corner point detection purpose in these experiments. The laparoscope was inserted into the trainer through a 5-mm trocar and was held in place using a stand made of LEGO® bricks to eliminate hand tremor.

We used the calibration results (O_{EMS_1}, O_{IMG}, Initial Calibration, Initial Pose) from one of the five freehand calibration trials in Experiment 1. We slightly rotated the camera head relative to the telescope, a few angles at a time, both clockwise and counterclockwise. After each rotation, a picture of the *fCalib* pattern was acquired and corner points were automatically detected from the picture. The rotation angle θ was calculated based on O_{EMS_1}, the Initial Pose, and the current pose (tracking data of the two sensors). The rotation-corrected projection of corner points (p_{cor}) were obtained based on O_{IMG}, θ, and the Initial Calibration, and were compared with the detected corner points (p_{det}) using the RMS re-projection error, which is defined as

$$\text{error} = \sqrt{\frac{1}{N} \sum_{i=1}^{N} d\left(p_{cor}^i, p_{det}^i\right)^2} \tag{7}$$

where N is the number of detected corner points and $d\left(\cdot, \cdot\right)$ is the Euclidean distance in pixel. It is worth mentioning that the SIC method [15,16] will detect as many corner points as possible in any visible part of the calibration pattern.

Experiment 4

To further evaluate dynamic calibration accuracy for practical use, we visually examined the virtual tube overlay using the *fCalib* plate. A feature of *fCalib* is the ability to immediately check the calibration accuracy by overlaying a virtual tube model on the camera image [17]. We used this feature and overlaid the rotation-corrected virtual tube on the image. A good visual agreement between the virtual and the actual tubes shown in the image suggests accurate calibration and rotation correction.

Table 1 Results from Step 1 of the five freehand calibrations

	O_{EMS_1}[a] (mm)	Distance[b] (mm)
Calibration 1	(−32.6, −38.6, −7.8)	54.2 ± 0.6
Calibration 2	(−32.9, −38.5, −8.5)	53.8 ± 0.7
Calibration 3	(−32.1, −38.4, −8.0)	54.6 ± 0.6
Calibration 4	(−32.8, −38.4, −8.3)	53.9 ± 0.7
Calibration 5	(−33.0, −38.2, −9.0)	53.9 ± 0.7

[a] 3D rotation center in EMS$_1$'s (EM sensor on the telescope) coordinate system

[b] Distance from O_{EMS_1} to the collected sample points located on the circle centered at O_{EMS_1}

A team member performed calibration of the oblique laparoscope following the described procedure. The laparoscope was then inserted into the trainer along with two other surgical tools. The *fCalib* plate was also placed inside the trainer so that the tube could simulate a target structure such as blood vessel or bile duct. The team member rotated the two parts of the laparoscope by random angles both clockwise and counterclockwise. During the rotation, the team member held the telescope relatively stable and rotated the camera head such that the tube stayed in the field of view. The virtual tube model, generated before and after rotation correction, can be visualized in the video. To trigger rotation correction, the team member pressed a button using a foot pedal. After rotation correction, the team member moved the laparoscope around to visually assess the accuracy of the overlay between the actual and the virtual tubes shown in the video.

Results

Experiment 1

It took an average of 2 min and 8 s (range 1 min and 50 s–2 min and 25 s) to complete one calibration. Table 1 lists the results from Step 1 of the five calibration trials. It indicates the estimated O_{EMS_1} are consistent. Figure 6 shows the
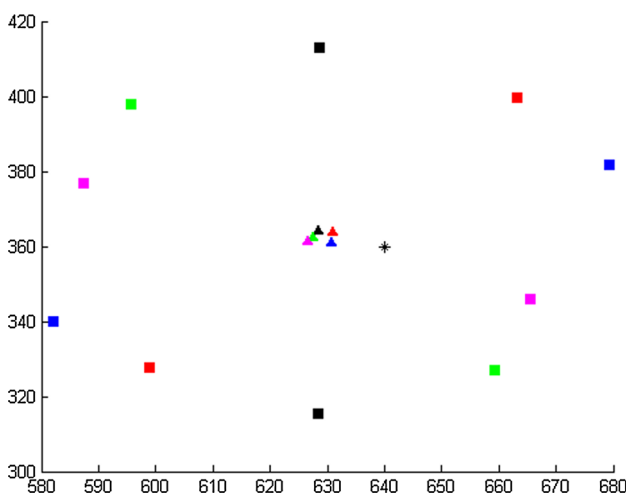
estimated principal points (two in each calibration), the calculated O_{IMG}, and the image center [i.e., (640, 360) in our case] as a reference. The actual rotation angles between the First and the Second Calibrations (the ideal angle is 180°) ranged from 176.5° to 179.7°. As can be seen, the calculated O_{IMG} was stable and differed considerably from the respective principal points and less so from the image center. Except for the varying principal points, other calibrated parameters such as the focal length and the distortion coefficient were consistent among different calibration trials and comparable to our previous results reported in [17]. The 10 SICs (two in each calibration) yielded 1.2 ± 0.2 pixel RMS re-projection error.

Experiment 2

Based on the results from Experiment 1, it is reasonable to assume the ground truth O_{IMG}^{ref} to be the average of the five calculated O_{IMG}. Let θ be the rotation angle between Pose 1 and Pose 2. Table 2 shows the distances from O_{IMG}^{ref} to: (1) O_{IMG} of the five calibrations in Experiment 1, (2) the image center, and (3) O_{IMG} of the three additional calibration trials in Experiment 2. The results suggest a rotation of $180° \pm 5°$ between Pose 1 and Pose 2 is necessary.

Experiment 3

Figure 7 shows the RMS re-projection error using our method (range 2.4–8.5 pixel). As a reference, we also showed the re-projection error with the approach using image center as the rotation center in the image. Combined with Table 2, it can
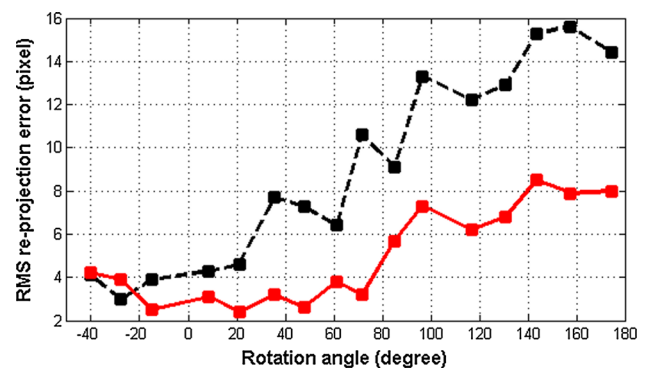

Fig. 6 Comparison of the rotation center in the image O_{IMG} (*triangle*), the principal points (*square*), and the image center (*star*). Each O_{IMG} was calculated using two principal points of the *same color*. The image resolution was 1280×720 pixels.

Fig. 7 RMS re-projection error comparing the rotation-corrected projection of corner points and the detected corner points. The *red solid line* is our method, whereas the *black dashed line* refers to the method using the image center as the rotation center in the image

Table 2 Distance from O_{IMG}^{ref} to O_{IMG} (with various θ) and image center		$\theta \in [175°, 185°]$	$\theta \approx 170°$	Image center	$\theta \approx 160°$	$\theta \approx 150°$
	Distance (pixel)	[1.4, 2.6]	7.7	11.3	12.4	16.1

θ = −40.3°, RMS re-projection error = 4.2 pixel

θ = 61.0°, RMS re-projection error = 3.8 pixel
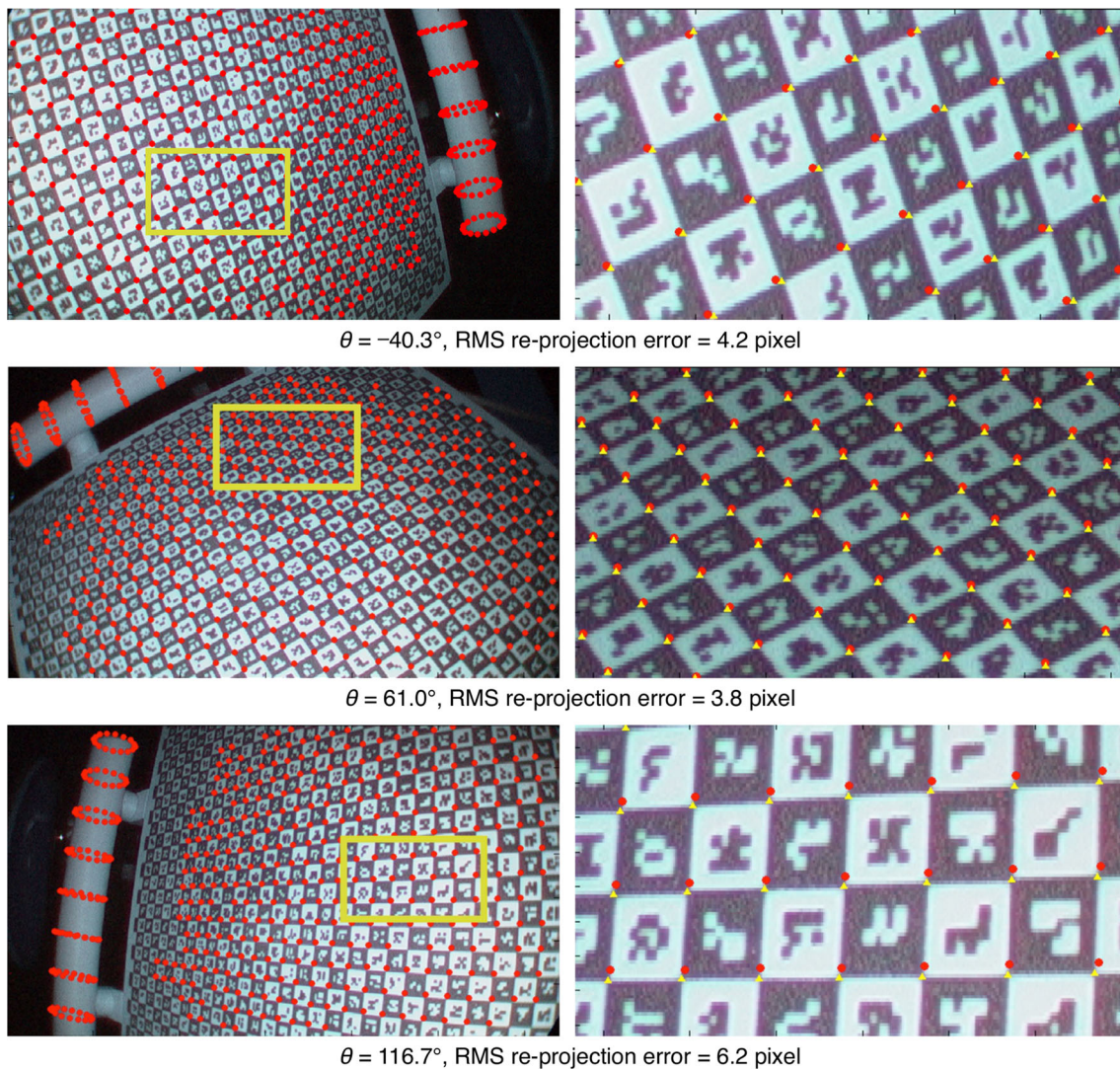
θ = 116.7°, RMS re-projection error = 6.2 pixel

Fig. 8 *Left* rotation-corrected projection of corner points superimposed on the original image. The *image* also shows the overlay of the rotation-corrected virtue tube (a *series of rings*) and the actual tube. *Right* close-up view showing the rotation-corrected projection of corner points (*red dot*) and the detected corner points (*yellow triangle*). As a reference, the physical size of the edge of each *square* in the *fCalib* pattern is 3.2 mm

be seen that more distance from O_{IMG}^{ref} yielded worse RMS re-projection error.

As a qualitative evaluation of our method's static accuracy, we superimposed rotation-corrected projection of corner points on the original images at three different rotation angles (Fig. 8). In the close-up views of Fig. 8, we showed the detected corner points and the rotation-corrected projection of corner points.

Experiment 4

A video clip showing handling of the laparoscope as well as the overlay of the virtual and the actual tubes has been supplied as supplementary multimedia material. Three sample

snapshots of the video are shown in Fig. 9. In general, there is good spatial agreement between the actual tube and the rotation-corrected virtual tube, and the correction came into effect in near real time after the button was pressed.

Discussion and conclusions

In this paper, we have reported a fast calibration method for oblique-viewing rigid endoscopes. In contrast to previous approaches, we used EM tracking as the external tracking hardware to improve the compactness and practicality of the system configuration. To enable OR use, single-image calibration was incorporated into the method and a sterilizable
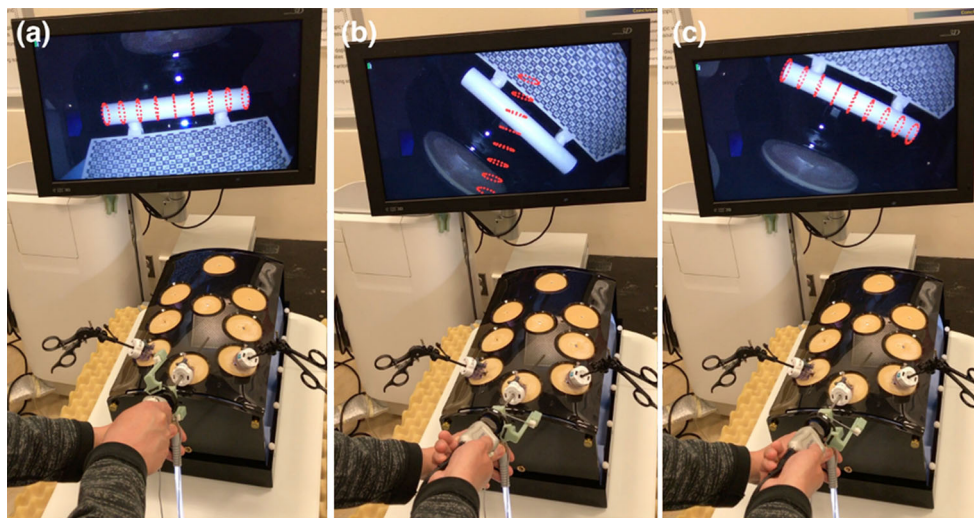
Fig. 9 Three snapshots of the submitted video clip. The video shows handling of the laparoscope as well as the overlay of the virtual and the actual tubes. **a** The initial state before rotation. **b** The laparoscope was rotated, and rotation correction in the image was not applied (before pressing the button). **c** Rotation correction in the image applied (after pressing the button)

plate, laser-marked with a calibration pattern, was developed. Furthermore, we proposed a universally accepted method to estimate the rotation center in the camera image without relying on image features that may or may not be present. The proposed method was validated both qualitatively and quantitatively in a simulated clinical environment.

One major advantage of our method is that it is a fast and easy calibration procedure that has the potential to be performed by the clinical staff in the OR. The process is expected to add about 2 min to the existing clinical workflow; however, it can be performed in parallel with the preparation of the CAS system that employs the oblique-viewing endoscope. Our future work will include training the clinical staff to perform and test our calibration method through animal and human experiments to examine the learning curve, the ease of use, the actual time spent, and the accuracy of the method in practical situations.

Our method constitutes an improvement on the Wu method [12] with a better estimation of the rotation center in the image O_{IMG}. It is worth mentioning that, other than using Eq. 2, it is possible to calculate the exact O_{IMG} based on the two principal points and the rotation angle. However, solving this problem mathematically would yield two possible solutions. One may consider using the distance to the image center as a criterion to choose from the two solutions. However, the differences among the principal point, the image center and O_{IMG} could vary from endoscope to endoscope. Investigating more types of endoscopes in the future would help us better understand these differences. Currently, our method is general enough for stable and accurate estimation of O_{IMG}.

For an approximate comparison of re-projection error reported in Fig. 7, Yamaguchi et al. [11] achieved less than

5 pixel re-projection error for a rotation in the [0°, 140°] range. Wu et al. [12] achieved a similar accuracy for angles within 75°; however, their re-projection error increased to 13 pixels when the angle increased to 100°. It should be noted that the image resolution in both these studies was less than or equal to 320 × 240, whereas the image resolution in our study is 1280 × 720, i.e., a 12-fold denser pixel matrix. In addition, our results compared more corner points on image periphery whereas the results in the above two studies compared only corner points close to the image center because their calibration pattern was the conventional checkerboard.

Wu et al. reported that the re-projection error increased greatly when the rotation angle increased beyond 75°. We observed a similar trend in our results: the error approximately doubled when the rotation angle exceeded 80°. A similar pattern was also presented in the results of the Melo work [15]. All the three methods are based on rotating the image plane to correct for the rotation offset. Thus, the error in the estimation of O_{IMG} appears to be one major contribution to the re-projection error. Another source of error is under- or overestimation of the rotation angle, which is calculated based on the estimated rotation center in 3D space O_{EMS_1} and the positions of the two EM sensors. As shown in Table 1, although x- and y-coordinates of O_{EMS_1} are quite stable, there is more variation in the estimated z-coordinate of O_{EMS_1}, which could cause small error in the estimation of O_{EMS_1}. Both of the errors in O_{IMG} and O_{EMS_1} will have a greater impact on larger rotation angles than smaller ones, causing the angle-dependent re-projection error as shown in Fig. 7. Nevertheless, based on the results shown in Fig. 8 and the accompanying video (Fig. 9), we do not anticipate rotation correction to fail using our method for larger rotation angles. In the unlikely event that the error turns out to

be unacceptable after a large rotation, re-calibration using
fCalib to reset the Initial Calibration and the Initial Pose con-
tinues to be an option. For example, in ultrasound-based AR
applications, the top edge of the overlaid ultrasound image
is expected to align with the bottom edge of the imaging
elements of the laparoscopic ultrasound transducer shown
in the video (from certain viewing perspectives). One can
re-initialize calibration if the alignment deteriorates signifi-
cantly after a large rotation.

In addition to rotation-related errors, there are also errors
resulting from EM tracking and the Initial Calibration. As
shown in the video (Fig. 9), the overlay error starts to change
direction (relative to the center line of the actual tube) when
the tube crosses the center of the camera image. This could
be an effect caused by both dynamic EM tracking error [18]
and the error in radial distortion estimation, which causes
extra inward or outward displacement of a point from its
ideal location. It should be noted that this phenomenon also
occurs for forward-viewing endoscopes.

In our current design of EM tracking mounts, 33.5° out of
360° of rotation angles cannot be reached because the track-
ing mount on the camera head blocks the light source cable.
An alternative option is to shorten the tracking mount on the
camera head so nothing restricts a complete 360-degree rota-
tion. However, this option will place the EM sensor closer to
the camera head and further from the FG, which could create
unacceptable EM tracking error. We favored better accuracy
over greater flexibility at this stage. Nevertheless, the major-
ity of rotation angles are still accessible and we anticipate
the small inaccessible angle range would not affect practical
use of the oblique-viewing endoscopes.

In conclusion, demonstrated in the laboratory setting, the
presented method enables fast and accurate calibration of
oblique-viewing rigid endoscope. Our work has the potential
to make such fast calibration possible in the actual clinical
setting as well and thus support clinical translation of many
emerging endoscopic CAS systems.

Compliance with ethical standards

Conflict of interest The authors declare that they have no conflict of
interest.

Informed consent Informed consent was obtained from all individual
participants included in the study.

Human participants This article does not contain any studies with
human participants or animals performed by any of the authors.

References

1. Tsai RY (1987) A versatile camera calibration technique for high-accuracy 3-D machine vision methodology using off-the-shelf TV cameras and lenses. IEEE J Robot Automat 3:323–344
2. Heikkila J, Silven O (1997) A four-step camera calibration procedure with implicit image correction. In: Proceedings of IEEE computer society conference computer vision pattern recognition, pp 1106–1112
3. Zhang Z (1999) Flexible camera calibration by viewing a plane from unknown orientations. In: Proceedings of international conference on computer vision, pp 666–673
4. Bouguet JY (2016) Camera calibration with OpenCV. http://docs.opencv.org/2.4/doc/tutorials/calib3d/camera_calibration/camera_calibration.html. Accessed 21 Nov 2016
5. Shiu Y, Ahmad S (1989) Calibration of wrist-mounted robotic sensors by solving homogeneous transform equations of the form ax = xb. IEEE Trans Bobot Autom 5(1):16–29
6. Feuerstein M, Mussack T, Heining SM, Navab N (2008) Intraoperative laparoscope augmentation for port placement and resection planning in minimally invasive liver resection. IEEE Trans Med Imaging 27(3):355–369
7. Shekhar R, Dandekar O, Bhat V, Philip M, Lei P, Godinez C, Sutton E, George I, Kavic S, Mezrich R, Park A (2010) Live augmented reality: a new visualization method for laparoscopic surgery using continuous volumetric computed tomography. Surg Endosc 24(8):1976–1985
8. Kang X, Azizian M, Wilson E, Wu K, Martin AD, Kane TD, Peters CA, Cleary K, Shekhar R (2014) Stereoscopic augmented reality for laparoscopic surgery. Surg Endosc 28(7):2227–2235
9. Cheung CL, Wedlake C, Moore J, Pautler SE, Peters TM (2010) Fused video and ultrasound images for minimally invasive partial nephrectomy: a phantom study. Proc Med Image Comput Comput Assist Interv 13(Pt 3):408–415
10. Liu X, Kang S, Plishker W, Zaki G, Kane TD, Shekhar R (2016) Laparoscopic stereoscopic augmented reality: toward a clinically viable electromagnetic tracking solution. J Med Imaging 3(4):045001
11. Yamaguchi T, Nakamoto M, Sato Y, Konishi K, Hashizume M, Sugano N, Yoshikawa H, Tamura S (2004) Development of a camera model and calibration procedure for oblique-viewing endoscopes. Comput Aided Surg 9(5):203–214
12. Wu C, Jaramaz B, Narasimhan SG (2010) A full geometric and photometric calibration method for oblique-viewing endoscopes. Comput Aided Surg 15(1–3):19–31
13. De Buck S, Maes F, D'Hoore A, Suetens P (2007) Evaluation of a novel calibration technique for optically tracked oblique laparoscopes. Proc Med Image Comput Comput Assist Interv 10(Pt 1):467–474
14. Feuerstein M, Reichl T, Vogel J, Traub J, Navab N (2009) Magneto-optical tracking of flexible laparoscopic ultrasound: model-based online detection and correction of magnetic tracking errors. IEEE Trans Med Imaging 28(6):951–967
15. Melo R, Barreto JP, Falcão G (2012) A new solution for camera calibration and real-time image distortion correction in medical endoscopy-initial technical evaluation. IEEE Trans Biomed Eng 59(3):634–644
16. Barreto JP, Roquette J, Sturm P, Fonseca F (2009) Automatic camera calibration applied to medical endoscopy. In: Proceedings of British machine vision conference, pp 1-10
17. Liu X, Plishker W, Zaki G, Kang S, Kane TD, Shekhar R (2016) On-demand calibration and evaluation for electromagnetically tracked laparoscope in augmented reality visualization. Int J Comput Assist Radiol Surg 11(6):1163–1171

18. Franz AM, Haidegger T, Birkfellner W, Cleary K, Peters TM, Maier-Hein L (2014) Electromagnetic tracking in medicine-a review of technology, validation, and applications. IEEE Trans Med Imaging 33(8):1702–1725

19. Maier-Hein L, Franz AM, Birkfellner W, Hummel J, Gergel I, Wegner I, Meinzer HP (2012) Standardized assessment of new electromagnetic field generators in an interventional radiology setting. Med Phys 39(6):3424–3434

20. Liu X, Kang S, Wilson E, Peters CA, Kane TD, Shekhar R (2014) Evaluation of electromagnetic tracking for stereoscopic augmented reality laparoscopic visualization. In: Proceedings of MICCAI workshop on clinical image-based procedures: translational research in medical imaging, vol 8680, pp 84–91

21. Nijkamp J, Schermers B, Schmitz S, de Jonge S, Kuhlmann K, van der Heijden F, Sonke J-J, Ruers T (2016) Comparing position and orientation accuracy of different electromagnetic sensors for tracking during interventions. Int J Comput Assist Radiol Surg 11(8):1487–1498